Free-Vortex Flow Simulation Using a Three-Dimensional Euler Aerodynamic Method

P. Raj,* J. S. Sikora,† and J. M. Keen‡
Lockheed-California Company, Burbank, California

A three-dimensional Euler aerodynamic method based on a finite-volume, multistage time-stepping algorithm is used to simulate free vortices generated by flow separation along the edges of swept, slender wings at moderate to high angles of attack. Computed results for a cropped-delta wing, an arrow wing, and a strake-wing-body configuration are correlated with experimental data and, for cropped-delta wing, with predictions of other numerical methods also. The flow is impulsively started and the vortices are automatically captured. The following two issues are specifically addressed: 1) sensitivity of the solutions to artificial viscosity and 2) effect of grid density on the results. Relatively small changes in the subsonic solutions are noticed with variations in the magnitude of artificial viscosity parameters and grid density. The correlations presented here provide an added measure of confidence in computational simulations using the Euler equations. The present investigation also raises some new issues related to vortex instabilities.

Introduction

THE accurate computational simulation of three-dimensional flows dominated by the interaction of free vortices with lifting surfaces is of considerable interest to aircraft designers. Trailing wakes and leading-edge separated vortices are typical examples of free vortices. The leading-edge separated vortices are the subject of the present investigation. They form on the leeward side of swept slender wings of typical fighter aircraft at moderate to high angles of attack during low-speed flight or transonic maneuvering. Significant improvements in aerodynamic performance can be derived by careful generation and control of these vortices. At present, a designer has to rely on extensive and costly wind-tunnel tests for necessary data. Accurate, efficient, and reliable computational methods are needed to complement the experimental tests.

Research on free-vortex flow simulation has produced a number of computational methods. At one end of the spectrum are the vortex-lattice[1-4] and free-vortex-sheet (FVS) methods[5,6] based on linearized potential-flow formulation. In these methods, the vortices have to be explicitly modeled either indirectly using the suction analogy of Polhamus[7] or directly using distribution of singularities[4,5] whose final locations and strengths are iteratively determined. At the other end of the spectrum are field methods based on Reynolds-averaged Navier-Stokes equations[8] that provide an essentially complete fluid-dynamic model. The leading-edge vortices evolve naturally as a part of the solution of these equations. However, the available methods are not suitable for routine practical applications because of the exorbitant requirements of computational resources and the lack of a suitable universal turbulence model.

Recent advances in numerical algorithms to solve the Euler equations[9,10] provide an attractive and cost-effective alternative to using Navier-Stokes codes. Their ability to automatically capture regions of rotational flows has been demonstrated in several investigations.[11-15] In this paper, results for a cropped-delta wing, an arrow wing, and a strake-wing-body configuration are presented that specifically address two critical issues related to the use of the Euler codes: 1) the sensitivity of the solution to artificial viscosity and 2) effect of grid density on the results.

A Three-dimensional Euler Aerodynamic Method, TEAM, is used in the present investigation. Its algorithm is briefly outlined in the next section. Correlations of computed results with experimental data are presented in the Results and Discussion section.

Three-Dimensional Euler Aerodynamic Method

The TEAM code is based on the explicit multistage time-stepping, finite-volume algorithm proposed by Jameson et al.[9] to solve the inviscid mass, momentum, and energy conservation equations, commonly referred to as Euler equations. Only the basic features are highlighted in this section. Additional details can be found in Refs. 9, 10, 12, 14, 16, and 17.

In the present algorithm, the region surrounding a given configuration is subdivided into small hexahedral cells. These cells may, in principle, be constructed in any convenient manner; only the Cartesian coordinates of the cell vertices are required. The version of the code used in this investigation can accommodate cells arranged according to boundary-conforming C–H, C–O, O–O, or O–H topologies. The C–H topology is illustrated in Fig. 1; others may be analogously defined.

The semidiscrete approximations to the time-dependent Euler equations are integrated using a multistage time-stepping scheme. Convergence to steady state is typically achieved in a few hundred time steps using a pseudo-time-stepping approach

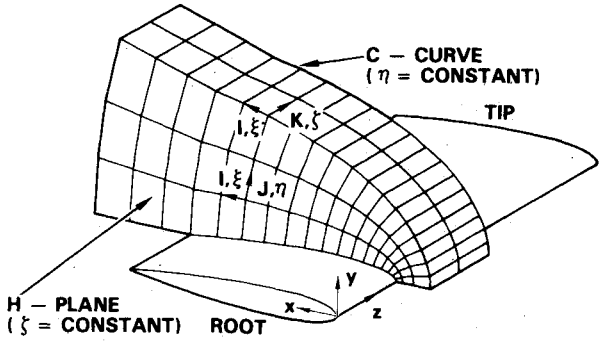

Fig. 1 C–H grid topology.

Received Oct. 14 1986; revision received May 26, 1987.

*R&D Engineer, Computational and Advanced Aerodynamics Department. Member AIAA.

†Senior Aerodynamics Engineer, Computational and Advanced Aerodynamics Department.

‡Aerodynamicist, Computational and Advanced Aerodynamics Department.

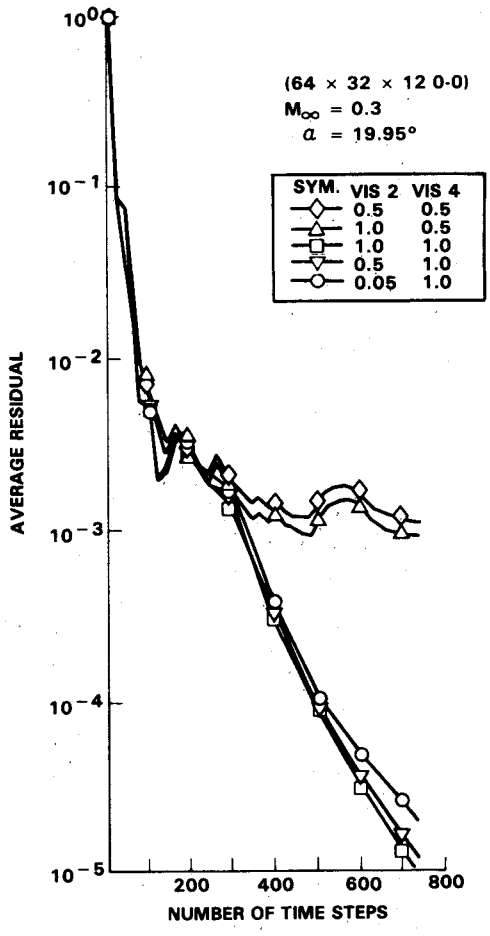

Fig. 2a Effect of numerical dissipation on rate of convergence for cropped-delta wing.

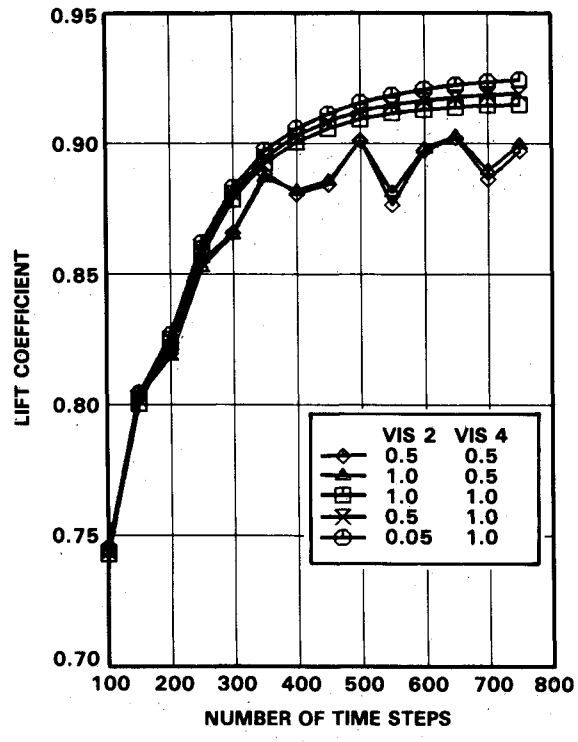

Fig. 2b Effect of numerical dissipation on lift coefficient convergence for cropped-delta wing.

in which the step size for each cell is determined by local stability restrictions. In contrast, thousands of steps are required when using a conventional explicit scheme with a global minimum-step size. Enthalpy damping and implicit residual smoothing further reduce the number of time steps required to reach the steady state. Appropriate nonreflecting conditions are used at the far-field boundaries. A no-normal-flow condition is imposed on the solid surface.

The independent variables—namely, density, Cartesian components of momentum, and total energy—are defined at cell centers, and the fluxes are computed at cell faces. This finite-volume spatial discretization reduces to a central-difference scheme that is formally second-order accurate for smooth grids. Adaptive dissipation terms (also known as artificial or numerical viscosity) are explicitly added to suppress the well-known tendency of central-difference schemes for odd-even point decoupling, to capture shocks automatically, and to minimize pre- and post-shock oscillations. The dissipation terms, composed of second and fourth differences, are constructed such that their values are small compared to those of the convective terms, except in some isolated regions. Therefore, possible contamination of an inviscid solution of the Euler equations is localized.

The user-specified coefficient (VIS-2) of the second-difference terms is scaled by the second derivative of static pressure. This introduces a larger amount of dissipation where it is most needed—near shocks and stagnation points—to suppress wiggles and overshoots. Elsewhere, their contribution is small. The fourth-difference terms are scaled by a user-input coefficient, VIS-4, divided by 64. These terms provide the necessary background dissipation to suppress the high-frequency error components and thereby minimize aliasing errors. They are turned off in regions where their values are smaller than those of the second-difference terms. The input values of VIS-2 and VIS-4 are typically of order one. Their effect on the solution was investigated in the present study, as discussed in the following section.

Results and Discussion

In this section, results computed using the TEAM code are correlated with experimental data for three cases: a cropped-delta wing, an arrow wing, and a strake-wing-body configuration. For each case, the entire domain is initialized to freestream conditions. This is equivalent to impulsively starting the flow. The Kutta condition is not explicitly applied. Pseudo-time stepping is used for all of the cases, and the variation of average residual with time steps is monitored to determine convergence to the steady state. The average residual refers to the root-mean-square value of the error in satisfying the mass-conservation equation. A four to five order-of-magnitude reduction in average residual is typically sufficient to obtain results that are accurate for engineering applications.

Cropped-Delta Wing

The cropped-delta wing has an aspect ratio of 0.87, a leading-edge sweep of 63 deg, and a taper ratio of 0.4. It is analyzed at 0.3 freestream Mach number and 19.95 deg angle of attack. All edges of this wing are sharp; therefore, the point of flow separation is unambiguously fixed at these edges. The results presented here illustrate the effect of varying the coefficients of the dissipation terms, as well as the grid density, on the solution.

Two O–O grids, a coarse one having 24,576 (64 × 32 × 12) cells and a fine grid with 110,592 (96 × 48 × 24) cells, are used. For the coarse grid, the wing is defined by 64 cells in the chordwise direction (32 each on the upper and lower surfaces) and 12 cells in the spanwise direction between the root and the tip. The corresponding numbers for the fine grid are 96 (48 each on the upper and lower surfaces) and 24. The grids were

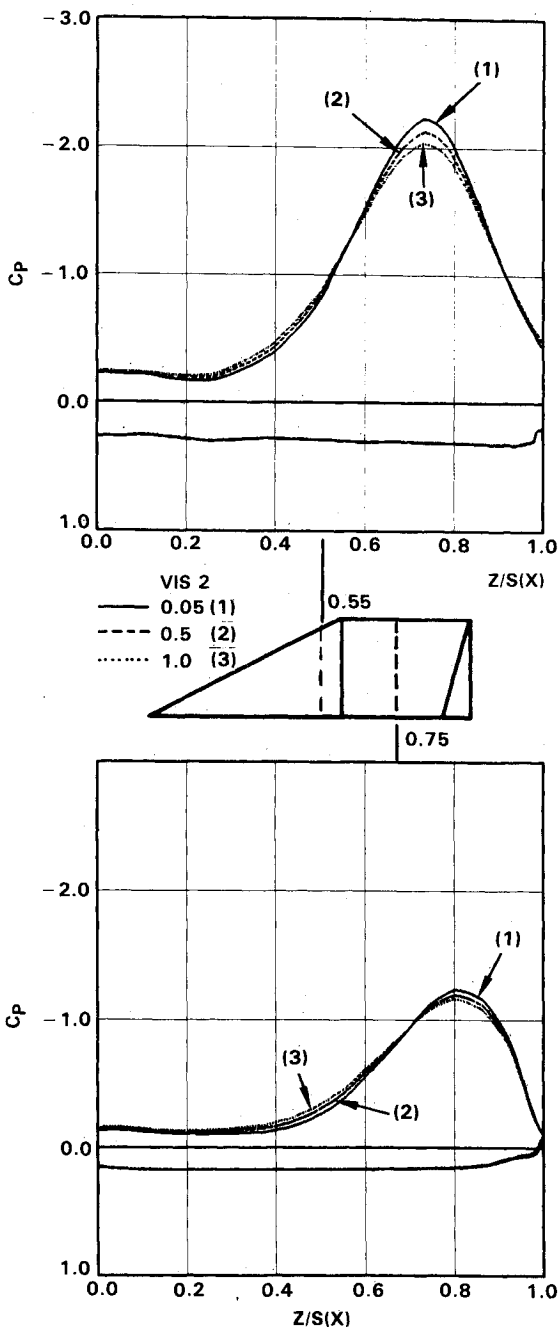

Fig. 3 Effect of VIS-2 variation (with VIS-4 fixed) on surface pressure distribution for cropped-delta wing.

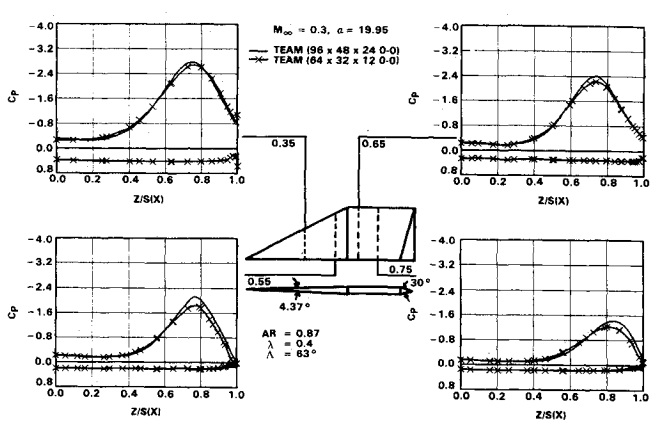

Fig. 4 Effect of grid density on surface pressure distribution for cropped-delta wing.

generated using the boundary integral grid (BIG) generation technique.[18]

The effect of changing the values of VIS-2 and VIS-4 on the convergence histories of average residual and lift coefficient for the coarse-grid analysis is shown in Figs. 2a and 2b, respectively. The dramatic impact of varying the value of VIS-4 is quite clear from these results. It was found that varying the values of VIS-2, although holding constant the value of VIS-4, led to rather small changes in the aerodynamic parameters, as well as the surface pressure distributions that are shown in Fig. 3. Of course, larger values of VIS-2 tend to diffuse the vortex.

To obtain the same level of convergence for the fine grid as for the coarse grid, the value of VIS-4 had to be increased to 3.0 while keeping VIS-2 fixed at 0.05. This reflects the effect of reduced cell size that decreases the magnitude of the fourth-difference terms. Computed cross-plane surface pressure distributions for the two grids are compared in Fig. 4. Increasing the number of cells results in a better resolution of the flowfield. However, the differences between the coarse- and fine-grid solutions are relatively small. The coarse-grid results provide a good engineering estimate.

In Fig. 5, the cross-plane surface pressure distributions computed using the TEAM code are correlated with the predictions of the FVS code, conical theory, and measured data of Luckring et al.[6] In general, the TEAM results are in good agreement with those of the FVS code. Since the latter has no numerical viscosity, the present correlations confirm that the numerical viscosity in TEAM has not significantly corrupted the global features of this inviscid solution to the Euler equations. Both TEAM and FVS fail to capture the secondary vortices whose presence is strongly suggested by the experimental data. This absence of secondary vortices in the computed results is primarily responsible for the lateral shift between the computed and the measured pressure peaks.

The correlations for this wing demonstrate the ability, as well as the limitations, of the inviscid TEAM code to simulate the free vortices resulting from the flow separation along sharp leading edges at high angles of attack and low Mach numbers. It must be noted that the free vortices are automatically captured by the TEAM code, whereas the FVS code requires their explicit modeling.

Arrow Wing

An arrow wing with an aspect ratio of 1.4, a leading-edge sweep of 71.2 deg, and a taper ratio of 0.1 is the second case. The wing is composed of airfoil sections that are approximately 3% thick. Both round leading-edge (RLE) and sharp leading-edge (SLE) sections were considered. Computations were carried out at subsonic and transonic Mach numbers using three O–O grids, two coarse and one fine, that were generated using the BIG code.[18] The two coarse grids had approximately the same total number of cells but different distributions. One of these with 24,576 (64 × 32 × 12) cells provided a denser grid in

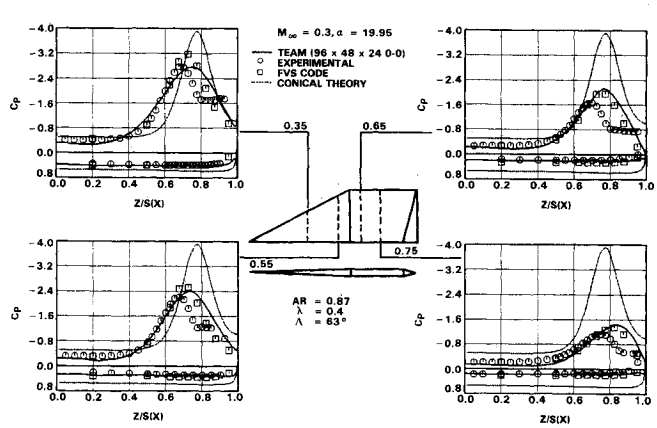

Fig. 5 Correlations of computed and measured cross-plane surface pressure distributions for cropped-delta wing.

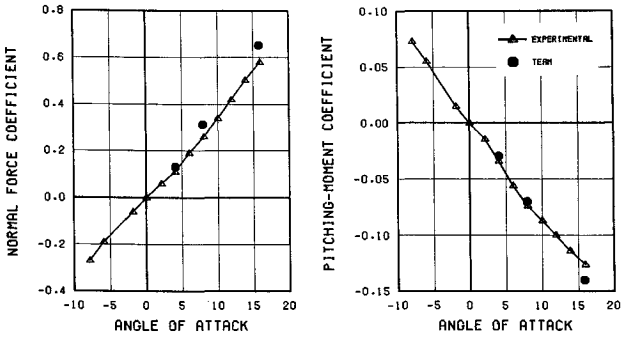

Fig. 6 Correlation of computed and measured aerodynamic parameters for arrow wing with round leading edge.

the vortex region, as compared to the other with 24,320 ($76 \times 20 \times 16$) cells. Note that the grid distribution for one of these grids is identical to that of the cropped-delta wing just discussed. The fine grid contained 109,440 ($96 \times 38 \times 30$) cells.

In Fig. 6, computed aerodynamic parameters for the round leading-edge wing using the fine grid at 0.85 freestream Mach number and at angles of attack of 4.0, 7.9, and 15.8 deg are correlated with experimental data.[19] The overall agreement is fairly good. The absence of body effect in the computations may be one of the sources of discrepancy. The wind-tunnel test was for a wing-body configuration, and the experimental data shown in this figure correspond to the integrated values using measured pressures on the wing. In addition, the viscous effects are not included in the present analysis. For the 15.8 deg angle-of-attack computation, fairly good agreement is obtained between the computed cross-plane pressure distributions and the experimental data, as shown in Fig. 7.

To investigate the effect of the leading-edge shape, computed cross-plane pressure distributions for the RLE and SLE wings were compared. For both of the wings, the computed results using the coarse grid differed from those using the fine grid. However, the effect of leading-edge shape was found to be rather localized to the leading-edge region when the computed results for RLE and SLE wings using a coarse (or fine) grid were compared with each other.[20] The experimental data also show the minimal effect of the leading-edge shape on the flowfield. Further study is required in light of recent investigations[21,22] in which the results for round-edge configurations are found to be sensitive to variations in grid density and numerical dissipation.

The sensitivity of the solution to grid density was investigated for the sharp leading-edge wing. Cross-plane surface pressure distributions at 0.85 Mach number and 15.8 deg angle of attack are correlated with experimental data in Fig. 8. The results show considerable dependence on the grid density. Both of the coarse-grid results are closer to each other but differ from the fine-grid solution. This reflects the inadequacy of the coarse grid to model a flow that is quite complex due to the possible interaction of shocks and free vortices. The subsonic-flow results shown in Fig. 9 exhibit much less sensitivity to grid density, as illustrated by the solutions for $64 \times 32 \times 12$ coarse grid and $96 \times 38 \times 30$ fine grid. Similar observations were made for the cropped-delta wing. However, the clustering of grid points could be crucial when coarse grids are used, as shown by the results in this figure. The distribution of cells between the wing and the far-field boundary in the $64 \times 32 \times 12$ grid is better able to resolve the vortex region than that for the $76 \times 20 \times 12$ grid. Therefore, the solution using the former is in relatively close agreement with the fine-grid solution compared to that for the latter.

The results presented here demonstrate TEAM's ability to model the free vortex flow at transonic Mach numbers. However, the transonic solutions exhibit considerable dependence on grid density. Additional studies using still denser grids are required to fully validate the code.

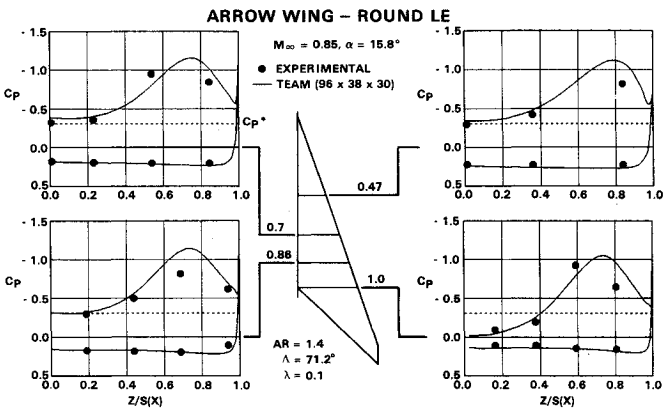

Fig. 7 Correlation of computed and measured cross-plane surface pressure distributions for arrow wing with round leading edge.

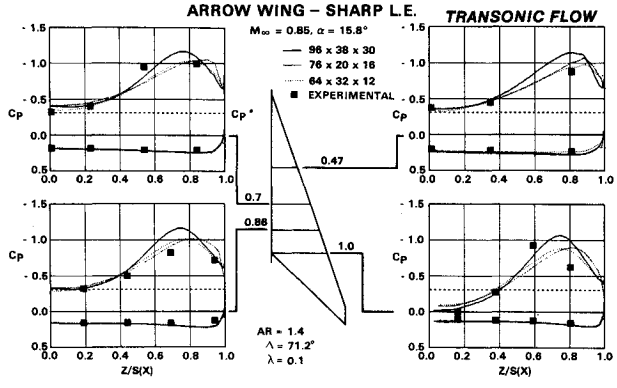

Fig. 8 Transonic flow correlations of computed and measured cross-plane surface pressure distributions for arrow wing with sharp leading edge.

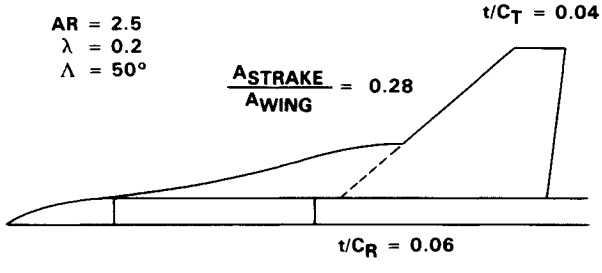

Fig. 10 Plan view of strake-wing-body configuration.

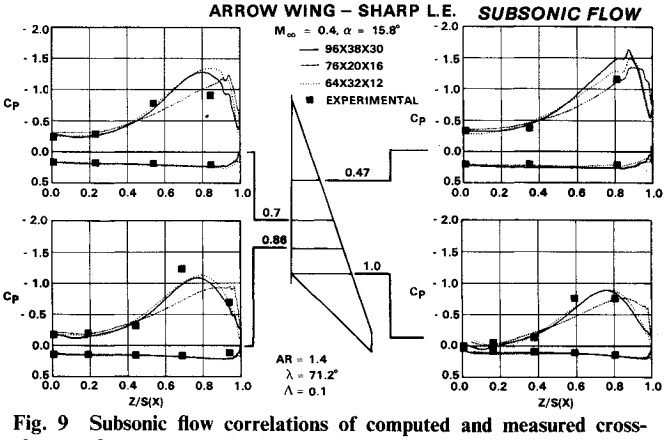

Fig. 9 Subsonic flow correlations of computed and measured cross-plane surface pressure distributions for arrow wing with sharp leading edge.

Strake-Wing-Body Configuration

The last set of results presented in this paper is for a strake-wing-body configuration[23] shown in Fig. 10. The wing has biconvex airfoils, and both the strake and wing have sharp leading edges. A $96 \times 32 \times 32$ C–H grid (98,304 cells) was used. The fuselage is treated as a bump on the plane of symmetry. There are 17 C curves between the strake-wing/body juncture and the body crown. The strake-wing (and wing itself for wing-body analysis) is defined by 60 cells (30 each on the upper and lower surfaces) in the chordwise direction and 22 cells in the spanwise direction between the root and the tip sections.

Values of computed lift coefficient for a strake-on configuration at a freestream Mach number of 0.5 are compared with experimental data[23] in Fig. 11. Two observations deserve mention here. The first one is that a steady-state solution could not be obtained for the 30 deg angle-of-attack case, whereas the average residual decreased by four to five orders of magnitude for other cases, as shown in Fig. 12. Different values of numerical dissipation coefficients did not affect this lack of convergence. The second observation relates to the large discrepancy between the computed and measured lift coefficients at angles of attack higher than 20 deg.

In regard to the first observation, a closer examination of the flowfield revealed the cause of this unsteadiness to be a localized vortex instability. It is illustrated in Fig. 13 by the flowfield at three cross-plane stations for three different values of time steps in the solution process. The flowfield is essentially steady at the forward station, but it is not so for the aft stations. The level of instability increases as one approaches the trailing edge region. Since pseudo-time stepping was used, the unconverged solutions are not physically meaningful except perhaps in a qualitative sense. Similar behavior has been observed in the computational simulation of a cropped-delta wing[24] and a cranked-delta wing.[25,26] Time-accurate calculation suggests itself as an alternative for further analysis, but the associated prohibitive cost is the major obstacle at present. It is nevertheless interesting to note that this angle of attack falls in the region where the experimental data exhibit a sudden loss of lift that is typically associated with vortex-burst-type instability.

There are at least two possible sources of discrepancies between converged solutions at higher angles of attack and measurements. The first involves the vortices generated by the separation of boundary layer on the forebody at angles of attack higher than 15 deg. Their presence is confirmed by oil-flow patterns shown in Ref. 27. These vortices are not automatically captured by the inviscid Euler code. The second is the relatively sparse cell distribution away from the surface. With increasing angle of attack, the vortices move farther away from the strake-wing surface, where they cannot be adequately resolved due to the coarseness of the grid. Further analysis is continuing.

Correlation between the computed and measured values for strake-off configuration is also shown in Fig. 11. For this case,

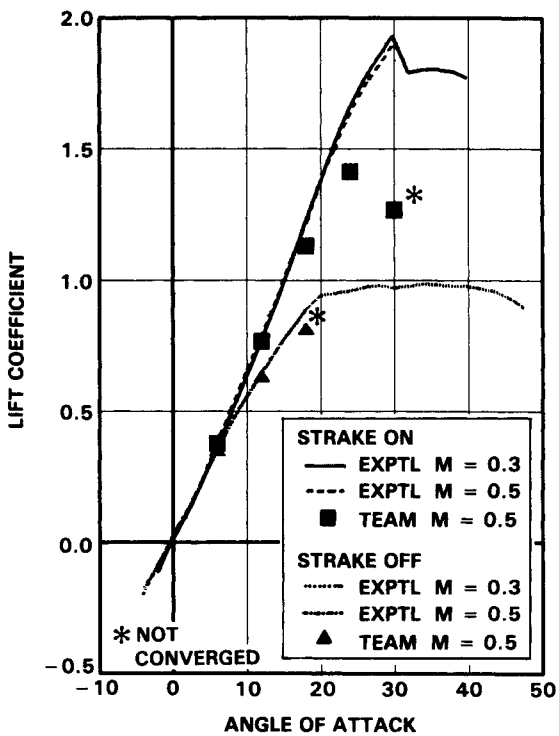

Fig. 11 Correlation of computed and measured lift coefficients for strake-on and strake-off configurations.

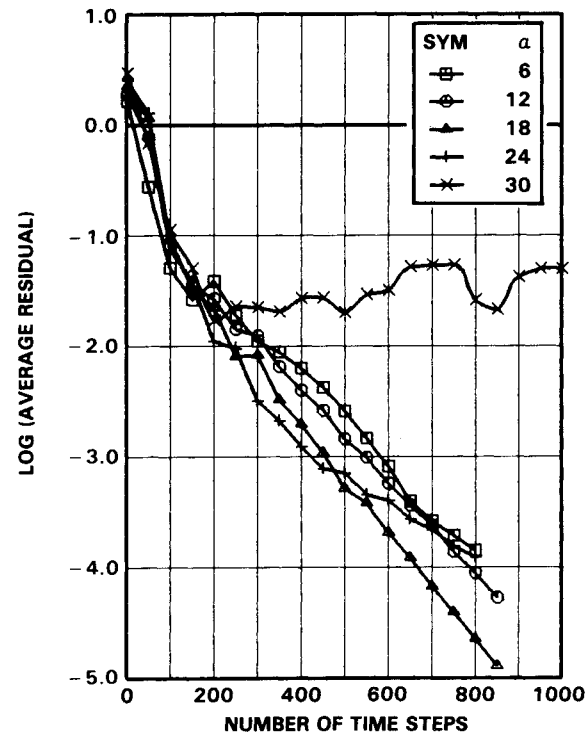

Fig. 12 Convergence history for strake-on configuration analysis.

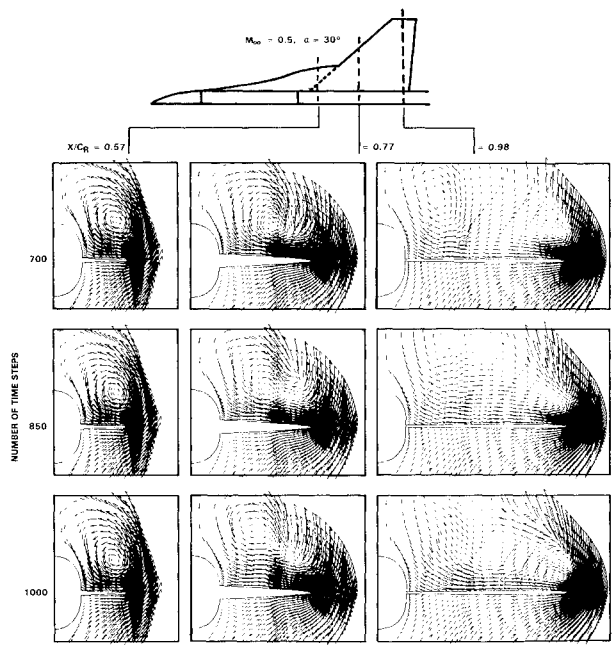

Fig. 13 Localized vortex instability for strake-on configuration.

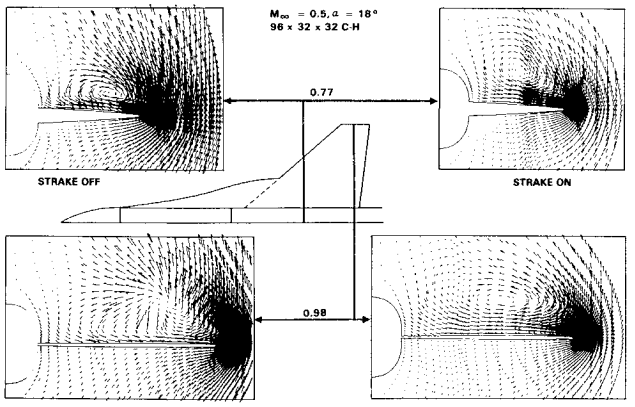

Fig. 14 Comparison of cross-plane flowfields for strake-on and strake-off configurations.

a steady-state solution could not be obtained for the 18 deg angle-of-attack case. The cross-plane flowfields presented in Fig. 14 illustrate the source of this unsteadiness as a vortex instability over the aft part of the wing. The corresponding strake-on solution does not exhibit this instability.

Vorticity and Numerical Dissipation

The appearance of vorticity in the steady-state solutions of the Euler equations presented here may be puzzling at first glance since the differential equations are inviscid. However, one possible source of vorticity is contained in Crocco's theorem[28] that relates gradients of entropy, or total pressure, to gradients of vorticity for inviscid compressible flows. For computed flows containing captured shocks of variable strength, the shocks provide an obvious source of entropy gradients. Of course, the explicitly added numerical dissipation terms are crucial for capturing these shocks. Even for flows without shocks, the numerical dissipation can produce significant total pressure losses (or entropy gradients) in certain regions containing large flow gradients, e.g., near stagnation points. Inaccuracies related to the numerical implementation of the no-normal-flow boundary condition near sharp edges and regions of large curvature can further increase these losses.

Based on the results presented in this paper and other investigations by the authors, it may be concluded that the generation of vortices about sharp-edged wings due to the total pressure losses is quite insensitive to the actual magnitude of the numerical dissipation, *as long as there is some*. It is not, however, very surprising, considering the observed Reynolds-number independence of a large class of leading-edge vortex flows for slender wings with sharp edges. Other recent investigations[21,26] have led to similar observations.

Interpretation of separated-flow results for wings with rounded edges requires more caution. The total pressure losses due to numerical dissipation depend on grid density, user-specified coefficients, and flow gradients.[21] Results for the arrow wing presented here and similar results of Hitzel and Schmidt[11] suggest that the Euler solutions may provide meaningful data as long as the radius of curvature is relatively small. Further investigation is required to provide useful guidelines to airplane designers.

Concluding Remarks

The correlations shown in this paper illustrate the capability of the TEAM code to capture vortices resulting from flow separation along the leading edges and side edges of swept, slender wings at moderate to high angles of attack. Unlike the procedures based on velocity potential, such as the free-vortex-sheet technique, it is not required to explicitly model the vortices. They appear automatically wherever the flow requires them.

Based on the experience to date, the following observations related to the effect of numerical dissipation and grid density may be made.

1) Relatively large amounts of fourth-difference dissipation may be required to obtain converged solutions when using dense grids. The results presented here and in other numerical experiments suggest that the effect of this dissipation on the accuracy of the solution is insignificant, as long as it stays small compared to the convective terms.

2) Input values for the coefficient of the second-difference dissipation terms should be small so that the regions of high gradients are properly captured but not unduly diffused.

3) Fine tuning of the dissipation coefficients is not required to obtain results of engineering accuracy. For most cases, acceptable results are obtained for sets of coefficients differing by factors of two to three.

4) Global features of computed free-vortex flows about sharp-edged wings are relatively insensitive to grid densities for subsonic flows. Of course, the flowfield is better resolved on finer grids. The same is not necessarily true for wings with round edges.

5) For certain flow configurations, the pseudo-time marching solutions do not reach a steady state because the free vortices exhibit local instabilities. This issue requires further investigation.

Use of Euler codes appears to be an attractive alternative to using the Navier-Stokes codes that require greater computational resources and suffer from empiricism of turbulence modeling. This is especially true for flows that are practically Reynolds-number-independent and whose primary features are not significantly altered by the vortices generated by separation of the boundary layer along smooth surfaces. With ongoing validation, the present approach promises to result in an effective method for simulating vortex-dominated high-angle-of-attack flows for engineering applications.

Acknowledgment

This investigation was entirely supported by the Lockheed-California Company's Independent Research and Development program. The development of the TEAM code used in this study was partially funded by a U.S. Air Force contract. The support and encouragement of L. R. Miranda, Manager, Computational and Advanced Aerodynamics Department, is gratefully acknowledged. Thanks are also due to J. M. Luckring of NASA-Langley Research Center for supplying data for the cropped-delta wing.

References

[1]Lamar, J. E., "Extension of Leading-Edge-Suction Analogy to Wings with Separated Flow Around the Side Edges at Subsonic Speeds," NASA TR R-428, Oct. 1974.

[2]Lamar, J. E. and Gloss, B. B., "Subsonic Aerodynamic Characteristics of Interacting Lifting Surfaces with Separated Flow Around Sharp Edges Predicted by a Vortex-Lattice Method," NASA TN D-7921, Sept. 1975.

[3]Lan. C. E. and Chang, J.-F., "Calculation of Vortex Lift Effect for Cambered Wings by Suction Analogy," NASA CR 3449, July 1981.

[4]Mehrotra, S. C. and Lan, C. E., "A Theoretical Investigation of the Aerodynamics of Low-Aspect-Ratio Wings with Partial Leading-Edge Separation," NASA CR-145304, 1978.

[5]Johnson, F. T., Lu, P., Tinoco, E. N., and Epton, M. A., "An Improved Panel Method for the Solution of Three-Dimensional Leading-Edge Vortex Flows," NASA CR-3273, July 1980.

[6]Luckring, J. M., Schoonover, W. E., and Frink, N. T., "Recent Advances in Applying Free Vortex Sheet Theory for the Estimation of Vortex Flow Aerodynamics," AIAA Paper 82-0095, Jan. 1982.

[7]Polhamus, E. C., "A Concept of the Vortex Lift of Sharp Edge Delta Wings Based on a Leading-Edge-Suction Analogy," NASA TN D-3767, 1966.

[8]Fujii, K. and Kutler, P., "Numerical Simulation of the Leading-Edge Separation Vortex for a Wing and Strake-Wing Configuration," AIAA Paper 83-1908-CP, July 1983.

[9]Jameson, A., Schmidt, W., and Turkel, E., "Numerical Solutions of

the Euler Equations by Finite-Volume Methods Using Runge-Kutta Time-Stepping Schemes," AIAA Paper 81-1259, June 1981.

[10]Rizzi, A., "Damped Euler Equation Method to Compute Transonic Flow Around Wing-Body Combinations," *AIAA Journal*, Vol. 20, Oct. 1982, pp. 1321–1328.

[11]Hitzel, S. M. and Schmidt, W., "Slender Wings with Leading-Edge Vortex Separation: A Challenge for Panel Methods and Euler Solvers," *AIAA Journal of Aircraft*, Vol. 21, Oct. 1984, pp. 751–759.

[12]Raj, P. and Sikora, J. S., "Free-Vortex Flows: Recent Encounters with an Euler Code," AIAA Paper 84-0135, Jan. 1984.

[13]Rizzi, A., "Computer Simulation of Non-Potential Flows Around Wings," *Aeronautical Journal*, Vol. 88, No. 876, June–July 1984, pp. 238–248.

[14]Raj, P., "Computational Simulation of Free-Vortex Flows Using An Euler Code," ICAS-84-1.3.1, 14th Congress of the International Council of the Aeronautical Sciences, Toulouse, France, Sept. 9–14, 1984.

[15]Rizzi, A. and Eriksson, L. E., "Computation of Inviscid Incompressible Flow with Rotation," *Journal of Fluid Mechanics*, Vol. 153, April 1985, pp. 275–312.

[16]Jameson, A. and Baker, T. J., "Solution of the Euler Equations for Complex Configurations," AIAA Paper 83-1929-CP, July 1983.

[17]Agarwal, R. K. and Deese, J. E., "Transonic Wing-Body Calculations Using Euler Equations," AIAA Paper 83-0501, Jan. 1983.

[18]Sikora, J. S. and Miranda, L. R., "Boundary Integral Grid Generation Technique," AIAA Paper 85-4088, Oct. 1985.

[19]Manro, M. E., Manning, K. J. R., Hallstaff, T. H., and Rogers, J. T., "Transonic Pressure Measurements and Comparison of Theory to Experiment for an Arrow-Wing Configuration," NASA CR-2610, Aug. 1976.

[20]Raj, P., Sikora, J. S., and Keen, J. M., "Free-Vortex Flow Simulation Using a Three-Dimensional Euler Aerodynamic Method," ICAS-86-1.5.2, 15th Congress of the International Council of the Aeronautical Sciences, London, England, Sept. 7–12, 1986.

[21]Newsome, R. W., "Euler and Navier-Stokes Solutions for Flow over a Conical Delta Wing," *AIAA Journal*, Vol. 24, April 1986, pp. 552–561.

[22]Kandil, O. A. and Chaug, A., "Numerical Dissipation Effect in Finite-Volume Euler Solutions for Conical Vortex-Dominated Flows," ICCM86-K.8, International Conference on Computational Mechanics, Tokyo, Japan, May 25–29, 1986.

[23]Luckring, J. M., "Subsonic Longitudinal and Lateral Aerodynamic Characteristics for a Systematic Series of Strake-Wing Configurations," NASA TM 78642, Feb. 1979.

[24]Raj, P. and Long, L. N., "An Euler Aerodynamic Method for Leading-Edge Vortex Flow Simulation," Vortex Flow Aerodynamics Conference, NASA-Langley Research Center, Oct. 8–10, 1985.

[25]Rizzi, A. and Purcell, C. J., "Numerical Experiment with Inviscid Vortex-Stretched Flow Around a Cranked Delta Wing: Subsonic Speed," AIAA Paper 85-4080, Oct. 1985.

[26]Murman, E. M. and Rizzi, A., "Applications of Euler Equations to Sharp Edge Delta Wings with Leading Edge Vortices," AGARD Symposium on Application of Computational Fluid Dynamics in Aeronautics, Aix-en-Provence, France, April 7–10, 1986.

[27]Luckring, J. M., "Flow Visualization Studies of a General Research Fighter Model Employing a Strake-Wing Concept at Subsonic Speeds," NASA TM 80057, Aug. 1979.

[28]Liepmann, H. W. and Roshko, A., *Elements of Gasdynamics*, Wiley, New York, 1957, p. 193.